Published in Proceedings of the National Academy of Sciences of the United States of America
Vol. 108, Issue 34, 2011, p. 14354-14359
which should be used for any reference to this work

Chloroplast lipid droplet type II NAD(P)H quinone oxidoreductase is essential for prenylquinone metabolism and vitamin K_1 accumulation

Lucia Eugeni Piller[a], Céline Besagni[a], Brigitte Ksas[b,c,d], Dominique Rumeau[b,c,d], Claire Bréhélin[e], Gaétan Glauser[f], Felix Kessler[a,1], and Michel Havaux[b,c,d]

[a]Laboratoire de Physiologie Végétale, Université de Neuchâtel, 2000 Neuchâtel, Switzerland; [b]Laboratoire d'Ecophysiologie Moléculaire des Plantes, Institut de Biologie Environnementale et de Biotechnologie, Service de Biologie Végétale et de Microbiologie Environnementale, Commissariat à l'Energie Atomique, 13108 Saint-Paul-lez-Durance, France; [c]Unité Mixte de Recherche Biologie Végétale et Microbiologie Environnementales, Centre National de la Recherche Scientifique, 13108 Saint-Paul-lez-Durance, France; [d]Université Aix-Marseille, 13108 Saint-Paul-lez-Durance, France; [e]Laboratoire de Biogenèse Membranaire, Unité Mixte de Recherche 5200, Centre National de la Recherche Scientifique, Université Bordeaux 2, F-33076 Bordeaux, France; and [f]Chemical Analytical Service of the Swiss Plant Science Web, Université de Neuchâtel, 2000 Neuchâtel, Switzerland

Lipid droplets are ubiquitous cellular structures in eukaryotes and are required for lipid metabolism. Little is currently known about plant lipid droplets other than oil bodies. Here, we define dual roles for chloroplast lipid droplets (plastoglobules) in energy and prenylquinone metabolism. The prenylquinones—plastoquinone, plastochromanol-8, phylloquinone (vitamin K_1), and tocopherol (vitamin E)—are partly stored in plastoglobules. This work shows that NAD(P)H dehydrogenase C1 (NDC1) (At5g08740), a type II NAD(P)H quinone oxidoreductase, associates with plastoglobules. NDC1 reduces a plastoquinone analog in vitro and affects the overall redox state of the total plastoquinone pool in vivo by reducing the plastoquinone reservoir of plastoglobules. Finally, NDC1 is required for normal plastochromanol-8 accumulation and is essential for vitamin K_1 production.

lipidomics | alternative electron flow | high light

Energy production in plants largely relies on oxygenic photosynthesis, implicating linear electron flow from water to NAD(P)H catalyzed by photosystems (PS) I and II. For optimal energy production, however, plants and algae have additional pathways, such as chlororespiration and cyclic electron transport around PSI, allowing the electrons to be recycled into the intersystem electron transport chain (1–4) (Fig. S1). In angiosperms, those alternative electron flows are mediated in part by the proton gradient regulation 5 (PGR5)/PGR5-like 1 (PGRL1) pathway and in part by a multisubunit NAD(P)H:plastoquinone oxidore-ductase (NDH) complex with similarity to bacterial and mito-chondrial Complex I (1, 5). Both the PGR5/PGRL1 pathway and the NDH complex have the ability to reduce plastoquinone (PQ) by using ferredoxin as the electron donor (6). A similar activity exists in the green alga *Chlamydomonas reinhardtii*, but this or-ganism does not encode the subunits of the NDH complex (7–9). Instead, a monomeric type II NAD(P)H:quinone oxidoreductase, NDA2, takes over the function of the NDH complex in cyclic electron flow and chlororespiration (10, 11). In *Arabidopsis thaliana*, seven such type II NAD(P)H dehydrogenase homologs are encoded by three subfamilies (12): two NDAs, four NDBs, and one NDC [termed NAD(P)H dehydrogenase C1 (NDC1)]. Their role, if any, in chloroplast electron pathways is not known. Interestingly, only *NDC1* appears to be of cyanobacterial origin (12). A study using GFP-fusion proteins initially localized all seven homologs in mitochondria (12). Later, NDC1 was imported into isolated mitochondria and also chloroplasts, suggesting a dual localization (13, 14). Furthermore, NDC1 was identified in proteomics studies of chloroplast lipid droplets (plastoglobules)(15, 16). The plastoglobules are a site of both prenylquinone metabolism and storage. Recently, a large reservoir of PQ, pro-bably not immediately involved in linear electron transport, was discovered in plastoglobules (17–19). Tocopherol (vitamin E), phylloquinone (vitamin K_1), and plastochromanol-8 (PC-8), a chromanol derivative of PQ, are also present in plastoglobules (15, 18–20) (Fig. S2).

Here, we demonstrate that NDC1 functions in a unique electron-flow pathway to the plastoglobule PQ reservoir and thereby determines the overall PQ redox state. Unexpectedly, NDC1 also plays a key role in plastochromanol accumulation and promotes the production of phylloquinone beyond its non-methylated 2-phytyl-1,4-naphthoquinone precursor.

Results

Chloroplast Lipid Droplet Localization of NDC1. Earlier studies suggested either a mitochondrial or dual mitochondrial/chloroplast localization for NDC1 (12–14). Two independent proteomics studies identified NDC1 as a chloroplast lipid droplet (plastoglobule) protein (15, 16). Sucrose-gradient flotation of total *Arabidopsis* chloroplast membranes followed by Western blotting demonstrated cofractionation of NDC1 with the plastoglobule markers PGL35 and PGL40 in the low-density fractions as well as the clear separation from the envelope marker Toc75 and the thylakoid marker LHCB2 (Fig. 1*A*). Transient expression of NDC1-YFP in *Nicotiana benthamiana* protoplasts resulted in punctate fluorescence mostly inside the chloroplasts (Fig. 1*B*). The punctate fluorescence, in most cases, colocalized with that of the neutral lipid dye Nile Red (Fig. 1*D*). These results are consistent with the lipid droplet/plastoglobule localization of NDC1 indicated by the earlier proteomic studies and the fractionation experiment (Fig. 1*A*). Nevertheless, both isolated chloroplasts (Fig. 1*F*) and mitochondria (Fig. 1*G*) imported synthetic, full-length [^{35}S]-labeled pre-NDC1 in vitro, resulting in protease-protected, mature forms in both cases.

Photosynthetic Parameters of the *ndc1* Mutant. We isolated two homozygous transfer-DNA insertion lines for the *NDC1* gene: Salk_024063 and GABI_614F03, named *ndc1-1* and *ndc1-3*, respectively. Immunoblotting with specific antibodies indicated the absence of the NDC1 protein and confirmed the homozygous

Author contributions: G.G., F.K., and M.H. designed research; L.E.P., C. Besagni, B.K., D.R., C. Bréhélin, G.G., and M.H. performed research; L.E.P., C. Besagni, and G.G. contributed new reagents/analytic tools; L.E.P., C. Besagni, D.R., G.G., F.K., and M.H. analyzed data; and F.K. wrote the paper.

The authors declare no conflict of interest.

[1]To whom correspondence should be addressed. E-mail: felix.kessler@unine.ch.

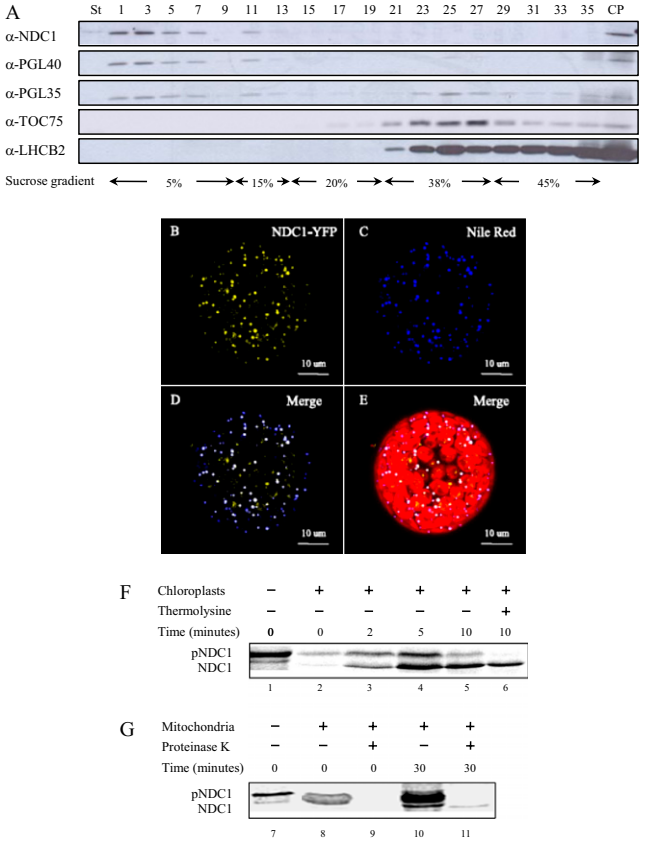

Fig. 1. NDC1 lipid droplet localization. (*A*) Western blotting of chloroplast membrane fractions separated by sucrose-gradient flotation. Toc75 and LHCB2 are envelope and thylakoid markers, respectively. PGL35 and PGL40 are plastoglobule markers. CP, total chloroplast; St, stroma. (*B*) NDC1-YFP under the control of the cauliflower mosaic virus 35S promoter was transiently expressed in tobacco protoplasts. Transformed protoplasts were analyzed by confocal laser microscopy. (*C*) The neutral lipid dye Nile Red reveals lipid droplets in chloroplasts (plastoglobules). (*D*) The first merged image shows the superposition of NDC1-YFP and Nile Red in white. (*E*) The second merged image shows the chlorophyll autofluorescence to visualize chloroplasts. (*F*) ^{35}S-labeled pre-NDC1 (lane 1) was incubated with isolated chloroplasts in vitro in a time-course experiment (0, 2, 5, and 10 min, lanes 2–5). The imported, lower molecular mass NDC1 was resistant to exogenously added thermolysin protease (lane 6). (*G*) ^{35}S-labeled pre-NDC1 was incubated with isolated mitochondria in vitro (lane 7). The experiment was analyzed at the 0- and 30-min time points (lanes 8 and 10). The imported, lower molecular mass NDC1 was resistant to exogenously added proteinase K (lanes 9 and 11).

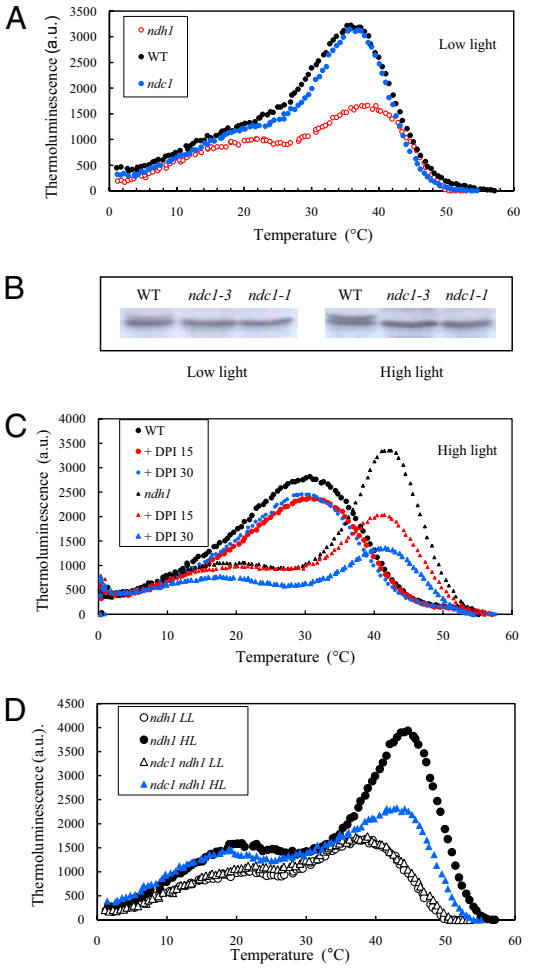

Fig. 2. Thermoluminescence measurements in WT, *ndc1*, and *ndh1* mutant leaves of *Arabidopsis*. (*A*) Far-red light-induced thermoluminescence signal in WT *Arabidopsis* leaves and in mutant leaves (*ndc1*, *ndh1*) grown under standard conditions. The band peaking at temperature >35 °C is the so-called afterglow band. The shoulder observed at lower temperature (~20 °C) is a B band corresponding to the $S_{2/3}$ Q_B− charge recombination. The data are representative traces of at least six separate experiments. (*B*) Immunodetection of NDC1 in total extracts of WT and two *ndc1* mutant lines (*ndc1-1* and *ndc1-3*) under normal and high-light growth conditions. The upper band, weakly visible in the WT under low-light conditions and more strongly under high-light conditions, corresponds to the NDC1 protein. The band is absent from the *ndc1-1* and *ndc1-3* mutants. The lower band is a nonspecific, cross-reacting signal. (*C*) Effects of DPI (15 and 30 μM) on the afterglow thermoluminescence band of WT and *ndh1* mutant leaves acclimated for 7 d to high light. Data are representative traces of three separate experiments; (*D*) Afterglow thermoluminescence band measured in leaves of the *ndh1* mutant and the *ndc1 ndh1* mutant acclimated for 7 d to high light. Data are representative traces of at least six separate experiments.

knockout nature of the two mutants (Fig. S3*A*). Neither of the lines had a visible phenotype (Fig. S3*B*).

We measured several chlorophyll fluorescence parameters in WT and *ndc1-1* leaves (hereafter called *ndc1*) and also, for comparison purposes, in leaves of the *ndh*o mutant (hereafter called *ndh1*) lacking the NDH complex (21): the maximal quantum yield of PSII photochemistry (F_v/F_m) was determined in the dark, whereas the actual PSII quantum yield ($\Delta F/F_m'$) and the nonphotochemical quenching of chlorophyll fluorescence were measured at different photon flux densities (PFDs) (Fig. S4 *A* and *B*). None of those parameters differed between WT and the *ndc1* mutant. We also analyzed alternative electron flows, which donate electrons from the stroma to the PQ pool, by using measurements of chlorophyll fluorescence (Fig. S4*C*), P700 redox state (Fig. S4*D*), and chlorophyll thermoluminescence (Fig. 2). The postillumination rise in chlorophyll fluorescence, which is indicative of PQ and primary quinone acceptor (Q_A) reduction specifically mediated by the NDH complex (21), remained unchanged in *ndc1* compared with WT (Fig. S4*C*). We also mea-sured the postillumination reduction of oxidized P700, the PSI reaction center pigment (22). Although a slight increase in the half life ($t_{½}$) of P700 reduction was observed in the *ndh1* mutant, indicating a slowdown of the electron donation to P700, the *ndc1* mutation had no effect on this parameter (Fig. S4*D*). Fig. 2*A* shows the afterglow thermoluminescence band, induced by far-red preillumination, that corresponds to a heat-induced back electron transfer to the PQ pool in the dark (23). In *Arabidopsis*, this pathway has been shown to reflect mainly the NDH activity (24, 25), as confirmed here by the strong reduction of this band in *ndh1*. Again, no difference was found between WT and *ndc1*.

From those results, we can conclude that NDC1 and NDH do not fulfill a similar function, and therefore NDC1 is probably not directly involved in cyclic or chlororespiratory electron flows (Fig. S1) under standard growth conditions.

We also analyzed plants previously exposed to high-light conditions that induce accumulation of plastoglobules (26) and increase expression of the *NDC1* gene in the WT (Fig. 2*B*) and *ndh1* mutant (Fig. S5) (27). In WT, high light shifted the afterglow band toward lower temperatures compared with low light (Fig. 2 *A* and *C*). This band shift is indicative of an activation of the cyclic electron pathway: electrons are rapidly transferred to the secondary quinone acceptor (Q_B) at room temperature, leading to charge recombination between Q_B^- and the S states and to the merging of the afterglow band with the B band (28, 29). This activation was not observed in *ndh1* mutant leaves. Rather surprisingly, high light induced the appearance of a unique band in this mutant, peaking at ~42 °C (Fig. 2 *C* and *D*). This band was insensitive to antimycin A (Fig. S6) but showed a high sensitivity to diphenyleneiodonium (DPI), a known inhibitor of type II NAD(P)H:quinone oxidoreductases (7) (Fig. 2*C*). Moreover, its amplitude was strongly reduced in the *ndc1 ndh1* double mutant (Fig. 2*D*), indicating the participation of NDC1 in this nonphotochemical electron flow.

In Vitro Activity of NDC1. NDC1 is a predicted NADH/NADPH:quinone reductase, and the thermoluminescence experiments supported such a role in vivo. For in vitro experimentation, purified recombinant NDC1 protein was incubated with NADPH as the electron donor and decyl-PQ (Fig. 3*A*). The decyl derivative is more soluble because of the replacement of the highly hydrophobic isoprenoid chain. We tracked the reactions by recording the oxidation of NAD(P)H at 340 nm. For decyl-PQ, we measured K_m = 9 μM and V_{max} = 46 μmol/mg per min (Fig. 3*A*). DPI inhibited decyl-PQ reduction in the presence of NAD(P)H with a half-maximal inhibition at ~2.5 μM (Fig. 3*B*). Isolated plastoglobules (Fig. 3*C*) and decyl-ubiquinone (with NADH as the electron donor) (Fig. 3*D*) also functioned as NDC1 substrates in vitro.

To determine how NDC1 affects prenyllipid levels in leaf extracts, we targeted PQ (Fig. 3 *E* and *F*), its derivative PC-8 (Fig. 3*G*), and α-tocopherol (Fig. 3*H*) for quantification by using HPLC coupled with UV and fluorescence detection systems. Neither tocopherol nor PQ were diminished in *ndc1* relative to WT. Interestingly, the PQ pool was substantially more oxidized in *ndc1* (50% oxidation) compared with WT (30% oxidation) (Fig. 3 *E* and *F*). Another striking result was the strong decrease of PC-8 in *ndc1* leaves (Fig. 3*G*). In contrast, the *ndh1* mutant did not show any significant change in the PQ redox state or in the PC-8 concentration.

Untargeted Lipidomic Analysis of the *ndc1* Mutant. To determine the more general role of NDC1 in chloroplast metabolism, we carried out untargeted lipidomics analyses (Fig. 4). Total lipid extracts of WT, *ndc1* (both *ndc1-1* and *ndc1-3*), *ndh1* single mutants, and the *ndc1 ndh1* double mutant were prepared and injected into an ultra HPLC–quadrupole time-of-flight mass spectrometer (UHPLC-QTOFMS). The data obtained were subjected to multivariate analysis to determine differences in lipid content between samples (Fig. 4*A*). Using principal component analysis, we observed two distinct groups (Fig. 4*A*): one containing WT and the *ndh1* mutant and the other containing the *ndc1* and *ndc1 ndh1* mutants. Principal component analysis loadings were then investigated and

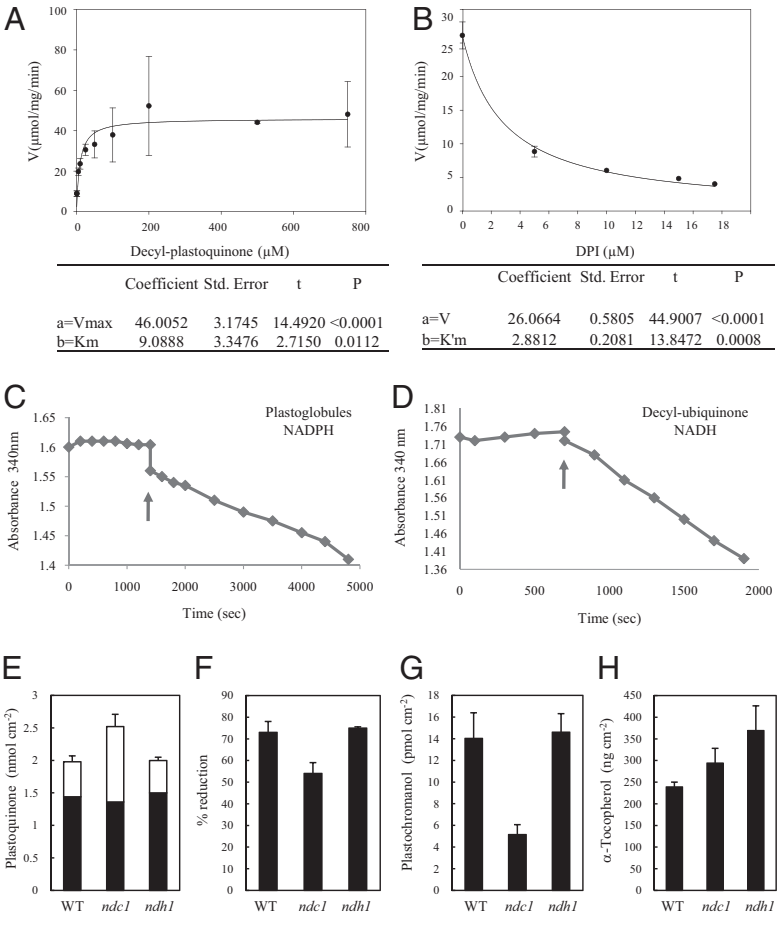

Fig. 3. NDC1 enzyme activity and prenylquinone quantification in the *ndc1* and *ndh1* mutants. (*A*) NDC1 activity was measured by monitoring NADPH oxidation in the presence of increasing concentrations of decyl-PQ (a PQ analog). (*B*) Increasing concentrations of the inhibitor DPI were added to the assay in the presence of 100 μM decyl-PQ. The kinetic parameters were calculated with SigmaPlot software. (*A* and *B*) Each data point represents two (*B*) and three (*A*) experimental replicates. (*C* and *D*) NDC1 activity was measured in the presence of isolated plastoglobules (*C*) and in the presence of decyl-ubiquinone and NADH (*D*). The arrows indicate the time point of addition of purified NDC1. (*E–H*) Prenylquinones in leaves determined by HPLC. (*E*) Total PQ. The white bar indicates the fraction of oxidized PQ. (*F*) Percentage reduction of the PQ pool. (*G*) PC-8. (*H*) α-Tocopherol in WT *Arabidopsis* leaves and *ndc1* or *ndh1* mutant leaves grown under standard conditions. Data are mean values of at least three separate experiments.

revealed that two variables were mostly contributive to the discrimination between both groups: *m/z* 450.3494 at 4.99 min for WT and *ndh1* and *m/z* 436.3336 at 4.64 min for *ndc*1 and *ndc1 ndh1* (Fig. 4*B* and Table S1). The ion at *m/z* 450.3494 was asso-ciated to the molecular formula $C_{31}H_{46}O_2$ (error = 0.9 ppm). A high-resolution MS/MS experiment gave a main fragment at *m/z* 185.0604, corresponding to the raw formula $C_{12}H_9O_2$ (error = 0.5 ppm) and a smaller fragment at *m/z* 225.0910 ($C_{15}H_{13}O_2$, error 2.7 = ppm). These molecular and fragment ions were typical of phylloquinone, a finding that was further confirmed by the in-jection of a standard compound that yielded identical mass spectra and eluted at identical retention times (Fig. S7). The ion at *m/z* 436.3336 corresponded to the molecular formula $C_{30}H_{44}O_2$ (error = 1.1 ppm) and could be caused by the demethylated form of phylloquinone (2-phytyl-1,4-naphthoquinone). The loss of a methyl group was confirmed by MS/MS, which generated a main fragment at *m/z* 171.0446 ($C_{11}H_7O_2$, error = 0.0 ppm) together with a smaller fragment at *m/z* 211.0760 ($C_{14}H_{11}O_2$, error = 0.5 ppm). No standard compound was available for this molecule, and the ion at *m/z* 436.3336 was thus tentatively annotated as 2-phytyl-1,4-naphthoquinone. The latter was further confirmed by using the *AtmenG* mutant known to accumulate 2-phytyl-1,4-naphthoquinone instead of phylloquinone (20): as in *ndc1*, the peak at *m/z* 436.3336 was present, whereas phylloquinone was almost absent (Fig. S7). Phylloquinone levels in the whole plant were statistically similar in WT and *ndh1* mutant with 2.76 and 3.23 μg/g of fresh weight (FW), respectively, whereas 2-phytyl-1,4-naph-thoquinone was almost completely absent from both lines (0.07 and 0.06 μg/g of FW in WT and *ndh1*, respectively). Conversely, in *ndc1* and *ndc1 ndh1* mutants, concentrations of phylloquinone were very low (0.02 and 0.05 μg/g of FW, respectively) and those of 2-phytyl-1,4-naphthoquinone were much higher, with 2.82 and 2.83 μg/g of FW, respectively. Interestingly, the levels of 2-phytyl- 1,4-naphthoquinone in *ndc1* and *ndc1 ndh1* mutants were similar to those of phylloquinone in WT and *ndh1* mutant (Fig. 4*C*).

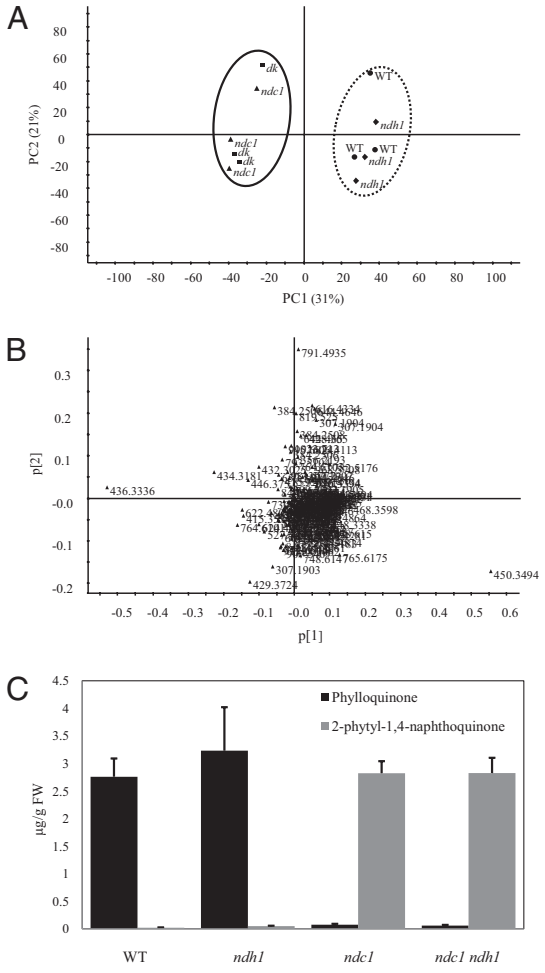

Fig. 4. Untargeted lipidomics of *ndc1* mutants. (*A*) Methanolic extracts from leaves of *ndc1*, *ndh1*, and *ndc1 ndh1* (*dk*) mutants lines were analyzed with UHPLC-QTOFMS. (*A*) Principal component analysis score plots (PC1 × PC2) with their percentages of explained variance, based on normalized data from negative ion UHPLC-QTOFMS analyses. (*B*) Corresponding loading plot showing the most relevant variables responsible for the separation found in the score plot (436.3336 on far left corresponds to 2-phytyl-1,4-naphthoquinone; 450.3494 on far right corresponds to phylloquinone). (*C*) Quantification of phylloquinone and 2-phytyl-1,4-naphthoquinone in WT (Col0) and *ndc1*, *ndh1*, and *ndc1 ndh1* mutant plants obtained from a standard solution of phylloquinone. Data represent the mean of two independent experiments (*n* = 3 each).

***AtMENG* Expression in the *ndc1* Mutant.** The absence of phylloquinone and its apparent replacement by the demethyl form in the *ndc1* mutant lines is surprising. It is known that AtMENG is re-quired for the final methylation step of phylloquinone bio-synthesis (20). We used RT-PCR to determine whether *AtMENG* is still expressed in the *ndc1* and *ndc1 ndh1* mutants (Fig. S8). We detected no significant differences in the *AtMENG* expression levels between the WT and the *ndc1*, *ndh1*, and *ndc1 ndh1* mutants, indicating that *AtMENG* is normally expressed in the mutant background and strongly suggesting that the active en-zyme is also present.

Discussion

This study supports the function of NDC1 in chloroplasts. In chloroplast fractionation experiments, NDC1 was almost exclusively detected in low-density plastoglobule-containing fractions (Fig. 1*A*). Moreover, NDC1-YFP fluorescence colocalized with Nile Red staining (mostly in chloroplasts), emphasizing its asso-ciation with lipid droplets (Fig. 1*D*). Nevertheless, this study also confirms in vitro import into both chloroplasts and mitochondria (Fig. 1 *F* and *G*) and does not exclude the dual localization of NDC1. A possible explanation for these apparently disparate findings is that NDC1 accumulates predominantly in chloroplasts and only at lower levels in mitochondria. A potential function in mitochondria was supported by the ability of purified, recombi-nant NDC1 to use decyl-ubiquinone together with NADH as a substrate (Fig. 3*D*). Overall, our observations favor the function of NDC1 in chloroplasts: although no effect on linear or cyclic electron transfer in chloroplasts was observed (Fig. S4), a unique afterglow thermoluminescence band (indicative of electron flow to PQ) appeared after highlight treatment of the *ndh1* mutant (Fig. 2). Its characteristics (insensitivity to antimycin A, sensitivity to DPI, and disappearance in the *ndc1 ndh1* double mutant) in-dicate that NDC1 functions in the chloroplast in a unique path-way of nonphotochemical PQ reduction parallel to cyclic and chlororespiratory electron flow (Fig. S1). Likely, this pathway corresponds to NDC1-catalyzed electron flow toward the PQ contained in the plastoglobules (17, 18) (Fig. S1). In support of this hypothesis, purified plastoglobules functioned as a quinone-containing substrate and accepted electrons from NADPH and the recombinant NDC1 enzyme in vitro (Fig. 3*C*). In agreement with this data, the PQ pool was significantly more oxidized in the *ndc1* mutant than in the WT (Fig. 3 *E* and *F*).

Decyl-PQ functioned as an in vitro substrate of recombinant NDC1 using NADPH as the electron donor (Fig. 3*A*). The ability of NDC1 to also use purified plastoglobules as a substrate was probably attributable to the PQ contained inside plastoglobules. This reaction may therefore reflect an in vivo scenario in which NDC1 binds to the plastoglobule surface thereby gaining access

to and reducing the PQ substrate inside and resulting in a higher overall reduction of the PQ pool in leaves.

This interpretation is in good agreement with the results of Kruk and coworkers (18, 30) who reported a large PQ reservoir that is not immediately implicated in photosynthesis and may be located in plastoglobules. Moreover, they proposed that this PQ reservoir plays a role as a lipid antioxidant in the thylakoid membrane. In such a scenario, NDC1 may function in the regeneration of reduced PQ upon oxidation, which would require the diffusion of PQ between plastoglobules and the thylakoid membrane, the compartment where PQ would likely function as an antioxidant in addition to its role as an electron carrier in photosynthesis. The diffusion of lipid compounds between plastoglobules and the thylakoid membranes has been proposed earlier, and physical connections between the outer lipid leaflet of the thylakoid membrane and the plastoglobule polar lipid monolayer were observed (17, 18, 26, 31).

Using HPLC and UHPLC-QTOFMS, we observed that the PC-8 concentration was strongly diminished in *ndc1* mutants (Fig. 3*G*). PC-8 is derived from PQ by the activity of VTE1, the tocopherol cyclase, present in the plastoglobule (18, 19, 32). For the cyclase to close the chromanol ring in dimethylphytylquinone (the precursor of γ-tocopherol) or in PQ, the quinol groups must preferentially be present in the reduced form (33). Thus, the reduction of PC-8 levels may reflect the redox state of the plastoglobule PQ reservoir, which is more oxidized than in WT. Interestingly, α-tocopherol was present at WT levels in the *ndc1* mutant, indicating that NDC1 is not required for its accumulation.

The untargeted lipidomics experiments led to unexpected discoveries (Fig. 4). The most prominent differences between WT and the *ndc1* mutants via UHPLC-MS were the almost complete absence of phylloquinone and the appearance of an additional peak corresponding in mass to the 2-phytyl-1,4-naphthoquinone, precursor of phylloquinone, in *ndc1* mutants. It is known that the complete absence of phylloquinone in *Arabidopsis* causes a lethal albino phenotype (34). However, in the *AtmenG* mutant (like in *ndc1*), its immediate precursor, 2-phytyl-1,4-naphthoquinone, still accumulates (20). Surprisingly, the *AtmenG* mutant has no visible phenotype, and it is therefore plausible that the 2-phytyl-1,4-naphthoquinone precursor functionally replaces phylloquinone. It is unclear why phylloquinone does not accumulate in the *ndc1* mutant. In RT-PCR experiments, *AtMENG* was expressed at the same level in both *ndc1* mutants and WT, suggesting that the enzyme is still present. However, AtMENG activity may be downregulated at the enzyme level, for instance, by the PQ redox state of the plastoglobules. Another possibility would be that, in the absence of NDC1, AtMENG is no longer correctly recruited to the site of its activity, which may implicate plastoglobules.

There are some indications that plastoglobules play a role in phylloquinone metabolism. A fraction of the total phylloquinone pool is present in the plastoglobules. In the *AtmenG* mutant, the 2-phytyl-1,4-naphthoquinone precursor of phylloquinone accumulated to a large extent in plastoglobules (20). Both the multiactivity protein PHYLLO and AtMENG gave punctate fluorescence when transiently expressed as GFP-fusion proteins in *Arabidopsis* protoplasts, suggesting a plastoglobule localization (20, 35).

In conclusion, NDC1 represents a unique electron input device for PQ. Unlike *C. reinhardtii* NDA2 (10, 11), it does not seem to be directly implicated in cyclic/chlororespiratory electron flows in thylakoids, but rather it plays a role in electron transfer to the plastoglobule PQ pool—a role that appears to be essential for prenylquinone metabolism.

Materials and Methods

Plant Materials and Growth Conditions. *Arabidopsis* plants were grown on soil (Ricoter) or in vitro on 0.8% phyto agar (Duchefa) containing 0.5× Murashige and Skoog medium (Duchefa) under short-day conditions (8 h light, 16 h dark, 150 $\mu mol \cdot m^{-2} \cdot s^{-1}$). For high-light experiments, plants aged 4 wk were acclimated for 7 d by increasing PFD to 750 $\mu mol \cdot m^{-2} \cdot s^{-1}$. Pea (*Pisum sativum*) seeds were germinated on soil after one night in water and grown in a chamber for 2 wk under a long-day conditions (16 h light, 8 h dark). *Nicotiana tabacum* cv. petit Havana plants used for protoplast isolation were grown for 4–5 wk on 0.5× Murashige and Skoog medium under long-day conditions.

Chlorophyll Fluorescence and Thermoluminescence. Chlorophyll fluorescence emission from attached leaves was measured with a PAM-2000 fluorometer (Walz) as previously described (21, 36). Thermoluminescence measurements were performed on leaf discs (1 cm in diameter) with a custom-made apparatus that has been described previously (24). The sample was cooled at 1 °C for 40 s, then it was illuminated for 30 s with far-red light (>715 nm, 3 $W \cdot m^{-2}$). Immediately after interrupting far-red illumination, temperature was increased from 1 °C to 70 °C at a rate of 0.5 $°C \cdot s^{-1}$, and luminescence was measured during heating with a photomultiplier tube.

Prenyllipid Quantification. Tocopherols, PQ (reduced and oxidized), and PC-8 were extracted, separated, and quantified by HPLC using the method described in refs. 18 and 30. The HPLC column was a Phenomenex C18 reverse-phase column (Kinetex, 2.6 μm, 100 × 4.6 mm).

P700 Redox Changes. The redox state of P700, the reaction center of PSI, was measured in attached leaves using a dual-wavelength emitter/detector ED-P700DW-E (Walz) connected to a PAM-101 unit, as previously described (8). P700 was oxidized by illuminating the leaf with far-red light (>715 nm, 25 $W \cdot m^{-2}$), and the rate of P700 reduction was measured in the dark after switching off the far-red light.

Chloroplast Fractionation and Western Blot Analysis. Chloroplast fractionation was carried out as described in ref. 14. Western blot analysis was carried out as described in ref. 14. Anti-NDC1 serum was used at 1/1,000 dilution on 5% milk/TBS.

In Vivo Targeting. Transient transformation of protoplasts was done by using the polyethylene glycol method (37, 38) with reduced cellulase (1%) and macerozyme (0.25%; Serva). Then, 20 μg of pEarlyGate101-NDC1-YFP was used to transform 500,000 tobacco protoplasts. Fluorescence was monitored with a Leica TCS SP5 confocal microscope at 48–80 h after transformation. Nile Red was used at 10 μg/mL (38).

In Vitro Import into Isolated Mitochondria and Chloroplasts. The radioactive full-length NDC1 protein was produced in a coupled transcription–translation system (TNT T7 Quick Coupled Transcription/Translation System; Promega) using pET21-NDC1-H6 vector according to the manufacturer's instructions. Import of [^{35}S]-labeled fusion protein into purified pea mitochondria was performed according to ref. 39. Import into purified *Arabidopsis* chloroplasts was performed according to ref. 40. All experiments were resolved by SDS/PAGE and analyzed by PhosphorImaging.

Production of Anti-AtNDC1 Antibody. Full-length recombinant NDC1-H_6 protein was purified under denaturing conditions by nickel nitrilotriacetic acid affinity chromatography (Qiagen) according to the manufacturer's recommendations. Polyclonal antibodies were produced in rabbit (Eurogentec) and were affinity-purified against NDC1-H_6 coupled to Affi-Gel 10 (Bio-Rad) according to the supplier's recommendations.

NDC1 Enzyme Assay. Activity was measured in 1 mL of 50 mM Hepes buffer [+KOH (pH 7.2)] containing 200 μM NADH and decyl-prenylquinone concentrations from 0.5 and 750 μM. The reaction was started by the addition of 18 μg of nickel nitrilotriacetic acid affinity-purified mature NDC1-H_6, and NADPH absorbance decay was measured at 340 nm.

Extraction and LC/MS Analysis. Plants (6-wk-old, $n = 6$) were ground to a fine powder under liquid nitrogen. Samples (100 mg) were extracted in 500 μL of MeOH for 2 min in a bead mill (MM 200; Retsch) and centrifuged (4 min at 14,000 × *g*), and the supernatant was recovered. The untargeted analysis of lipids was carried out with an Acquity UPLC system from Waters coupled to a Synapt G2 MS QTOF from Waters equipped with an atmospheric pressure chemical ionization source. The separation was performed at 60 °C on an Acquity BEH C18 column (50 × 2.1 mm, 1.7 μm) at a flow rate of 500 μL/min under the following conditions (A, water; B, MeOH): 80–100% B for 6 min, holding at 100% B for 3 min, followed by reequilibration at 80% for 2 min. The QTOF was operated at a resolution of 20,000 FWHM in MS positive

and negative ion modes over an *m/z* range of 225–1,200 in centroid mode. Scan time was 0.5 s. The corona current was set to 12 μA, and the cone voltage was set to 40 V. The source temperature was maintained at 120 °C, the atmospheric pressure chemical ionization probe was at 370 °C, and desolvation and cone gas flows were set to 800 L/hr and 20 L/hr, respectively. Accurate mass measurements (< 2 ppm) were obtained by infusing a solution of leucin-enkephalin at 400 ng/mL at a flow rate of 10 μL/min through the Lock Spray probe (internal calibration). MS/MS product ion spectra were obtained for phylloquinone and its demethylated form by using precursor ions at *m/z* 450.3 and 436.3, respectively. The collision energy was set to 25 eV, and argon was used as collision gas at a flow rate of 2.1 mL/min.

Absolute quantification of phylloquinone and 2-phytyl-1,4-naphthoquinone was performed with calibration curves obtained from standard solutions of phylloquinone at 100 ng/mL, 250 ng/mL, 1,000 ng/mL, and 2,500 ng/mL

Data Preprocessing and Multivariate Analysis. Peak picking and data processing including multivariate analysis were performed with MarkerLynx XS software (Waters), enabling the generation of a list of variables characterized by their *m/z*, retention time, and intensity. Peak areas of the extracted variables were normalized by dividing them by the sum of the intensities of all detected variables in each sample. Normalized variables were then Pareto-scaled and analyzed by principal component analysis.

Real-Time RT-PCR. Total RNA was extracted from Col0 control plants and mutant lines with the RNeasy Mini Kit (Qiagen). Then, 1 μg of total DNase-treated RNA was reverse-transcribed with the M-MLV reverse transcriptase (Promega). Real-time PCR was performed with SYBR Green (Thermo Scientific) on an iCycler with ACT2 as a reference. Specific primers to respective genes were as follows: *ACT2* forward, 5′-TGGAATCCACGAGACAACCTA-3′ and reverse, 5′-TTCTGTGAACG ATTCCTGGAC-3′); *AtMENG* forward, 5′- ATTCGATGCGGTTACGATGG-3′ and reverse, 5′- ACTCCTTTGCAAGATCATAAAC-3′; and *NDC1* forward, 5′-AGCTTGATTGGTGAAATGCC-3′ and reverse, 5′-CTGCGGTTATGCAGGAGTAG-3′.

ACKNOWLEDGMENTS. We thank Dr. Kruk for the kind gift of purified PQ standards. F.E.K. thanks the Université de Neuchâtel, SystemsX Plant Growth in a Changing Environment, and National Center of Competence in Research Plant Survival and acknowledges support from Swiss National Science Foundation Grant 31003A_127380.

1. Shikanai T (2007) Cyclic electron transport around photosystem I: Genetic approaches. *Annu Rev Plant Biol* 58:199–217.
2. Rumeau D, Peltier G, Cournac L (2007) Chlororespiration and cyclic electron flow around PSI during photosynthesis and plant stress response. *Plant Cell Environ* 30: 1041–1051.
3. Johnson GN (2011) Physiology of PSI cyclic electron transport in higher plants. *Biochim Biophys Acta* 1807:384–389.
4. Cardol P, Forti G, Finazzi G (2011) Regulation of electron transport in microalgae. *Biochim Biophys Acta* 1807:912–918.
5. Munekage Y, et al. (2002) PGR5 is involved in cyclic electron flow around photosystem I and is essential for photoprotection in *Arabidopsis*. *Cell* 110:361–371.
6. Yamamoto H, Peng L, Fukao Y, Shikanai T (2011) An Src homology 3 domain-like fold protein forms a ferredoxin binding site for the chloroplast NADH dehydrogenase-like complex in *Arabidopsis*. *Plant Cell* 23:1480–1493.
7. Mus F, Cournac L, Cardettini V, Caruana A, Peltier G (2005) Inhibitor studies on non-photochemical plastoquinone reduction and H_2 photoproduction in *Chlamydomonas reinhardtii*. *Biochim Biophys Acta* 1708:322–332.
8. Ravenel J, Peltier G, Havaux M (1994) The cyclic electron pathways around photosystem I in *Chlamydomonas reinhardtii* as determined in vivo by photoacoustic measurements of energy storage. *Planta* 193:251–259.
9. Peltier G, Cournac L (2002) Chlororespiration. *Annu Rev Plant Biol* 53:523–550.
10. Jans F, et al. (2008) A type II NAD(P)H dehydrogenase mediates light-independent plastoquinone reduction in the chloroplast of *Chlamydomonas*. *Proc Natl Acad Sci USA* 105:20546–20551.
11. Desplats C, et al. (2009) Characterization of Nda2, a plastoquinone-reducing type II NAD(P)H dehydrogenase in *Chlamydomonas* chloroplasts. *J Biol Chem* 284:4148–4157.
12. Michalecka AM, et al. (2003) *Arabidopsis* genes encoding mitochondrial type II NAD(P)H dehydrogenases have different evolutionary origin and show distinct responses to light. *Plant Physiol* 133:642–652.
13. Elhafez D, et al. (2006) Characterization of mitochondrial alternative NAD(P)H dehydrogenases in *Arabidopsis*: Intraorganelle location and expression. *Plant Cell Physiol* 47:43–54.
14. Carrie C, et al. (2008) Type II NAD(P)H dehydrogenases are targeted to mitochondria and chloroplasts or peroxisomes in *Arabidopsis thaliana*. *FEBS Lett* 582:3073–3079.
15. Vidi PA, et al. (2006) Tocopherol cyclase (VTE1) localization and vitamin E accumulation in chloroplast plastoglobule lipoprotein particles. *J Biol Chem* 281:11225–11234.
16. Ytterberg AJ, Peltier JB, van Wijk KJ (2006) Protein profiling of plastoglobules in chloroplasts and chromoplasts. A surprising site for differential accumulation of metabolic enzymes. *Plant Physiol* 140:984–997.
17. Bréhélin C, Kessler F (2008) The plastoglobule: A bag full of lipid biochemistry tricks. *Photochem Photobiol* 84:1388–1394.
18. Szymańska R, Kruk J (2010) Plastoquinol is the main prenyllipid synthesized during acclimation to high light conditions in *Arabidopsis* and is converted to plastochromanol by tocopherol cyclase. *Plant Cell Physiol* 51:537–545.
19. Zbierzak AM, et al. (2010) Intersection of the tocopherol and plastoquinol metabolic pathways at the plastoglobule. *Biochem J* 425:389–399.
20. Lohmann A, et al. (2006) Deficiency in phylloquinone (vitamin K_1) methylation affects prenyl quinone distribution, photosystem I abundance, and anthocyanin accumulation in the *Arabidopsis AtmenG* mutant. *J Biol Chem* 281:40461–40472.
21. Rumeau D, et al. (2005) New subunits NDH-M, -N, and -O, encoded by nuclear genes, are essential for plastid Ndh complex functioning in higher plants. *Plant Cell* 17: 219–232.
22. Maxwell PC, Biggins J (1976) Role of cyclic electron transport in photosynthesis as measured by the photoinduced turnover of P700 in vivo. *Biochemistry* 15:3975–3981.
23. Miranda T, Ducruet JM (1995) Characterization of the chlorophyll thermoluminescence afterglow in dark-adapted or far-red-illuminated plant leaves. *Plant Physiol Biochem* 33:689–699.
24. Havaux M, Rumeau D, Ducruet JM (2005) Probing the FQR and NDH activities involved in cyclic electron transport around Photosystem I by the 'afterglow' luminescence. *Biochim Biophys Acta* 1709:203–213.
25. Lintala M, et al. (2009) Comparative analysis of leaf-type ferredoxin-NADP oxidoreductase isoforms in *Arabidopsis thaliana*. *Plant J* 57:1103–1115.
26. Bréhélin C, Kessler F, van Wijk KJ (2007) Plastoglobules: Versatile lipoprotein particles in plastids. *Trends Plant Sci* 12:260–266.
27. Yoshida K, Noguchi K (2009) Differential gene expression profiles of the mitochondrial respiratory components in illuminated *Arabidopsis* leaves. *Plant Cell Physiol* 50: 1449–1462.
28. Ducruet JM, Roman M, Havaux M, Janda T, Gallais A (2005) Cyclic electron flow around PSI monitored by afterglow luminescence in leaves of maize inbred lines (*Zea mays* L.): Correlation with chilling tolerance. *Planta* 221:567–579.
29. Apostol S, Szalai G, Sujbert L, Popova LP, Janda T (2006) Non-invasive monitoring of the light-induced cyclic photosynthetic electron flow during cold hardening in wheat leaves. *Z Naturforsch C* 61:734–740.
30. Kruk J, Karpinski S (2006) An HPLC-based method of estimation of the total redox state of plastoquinone in chloroplasts, the size of the photochemically active plastoquinone-pool and its redox state in thylakoids of *Arabidopsis*. *Biochim Biophys Acta* 1757:1669–1675.
31. Austin JR, 2nd, Frost E, Vidi PA, Kessler F, Staehelin LA (2006) Plastoglobules are lipoprotein subcompartments of the chloroplast that are permanently coupled to thylakoid membranes and contain biosynthetic enzymes. *Plant Cell* 18:1693–1703.
32. Mène-Saffrané L, Jones AD, DellaPenna D (2010) Plastochromanol-8 and tocopherols are essential lipid-soluble antioxidants during seed desiccation and quiescence in *Arabidopsis*. *Proc Natl Acad Sci USA* 107:17815–17820.
33. Grütter C, Alonso E, Chougnet A, Woggon WD (2006) A biomimetic chromanol cyclization leading to α-tocopherol. *Angew Chem Int Ed Engl* 45:1126–1130.
34. Shimada H, et al. (2005) Inactivation and deficiency of core proteins of photosystems I and II caused by genetical phylloquinone and plastoquinone deficiency but retained lamellar structure in a T-DNA mutant of *Arabidopsis*. *Plant J* 41:627–637.
35. Gross J, et al. (2006) A plant locus essential for phylloquinone (vitamin K_1) biosynthesis originated from a fusion of four eubacterial genes. *J Biol Chem* 281: 17189–17196.
36. Havaux M, et al. (2009) Vitamin B6 deficient plants display increased sensitivity to high light and photo-oxidative stress. *BMC Plant Biol* 9:130.
37. Koop HU, et al. (1996) Integration of foreign sequences into the tobacco plastome via polyethylene glycol-mediated protoplast transformation. *Planta* 199:193–201.
38. Greenspan P, Mayer EP, Fowler SD (1985) Nile Red: A selective fluorescent stain for intracellular lipid droplets. *J Cell Biol* 100:965–973.
39. Moore AL, Fricaud AC, Walters AJ, Whitehouse DG (1993) Isolation and purification of functionally intact mitochondria from plant cells. *Methods Mol Biol* 19:133–139.
40. Agne B, et al. (2010) The acidic A-domain of *Arabidopsis* TOC159 occurs as a hyperphosphorylated protein. *Plant Physiol* 153:1016–1030.

Supporting Information

Eugeni Piller et al. 10.1073/pnas.1104790108

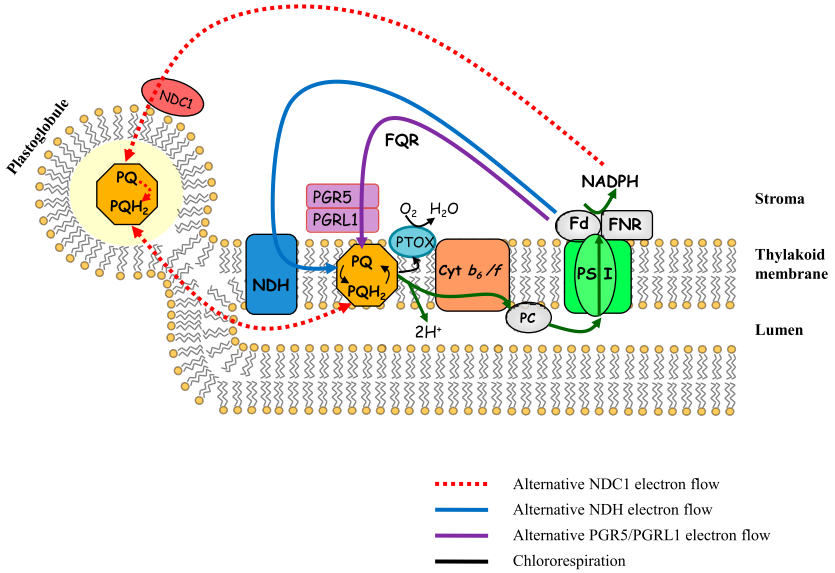

Fig. S1. Alternative electron-flow pathways. (*i*) proton gradient regulation 5 (PGR5)/PGR5-like 1 (PGRL1) pathway and (*ii*) the NAD(*P*)H:plastoquinone oxidoreductase (NDH) complex transfer electrons from ferredoxin (Fd) back to the thylakoid plastoquinone pool (PQ/PQH_2). These two processes contribute to cyclic electron flow around photosystem I (PSI). Chlororespiration involves transfer of electrons from PQH_2 directly to molecular oxygen via the plastid terminal oxidase (PTOX). NDC1 transfers electrons from NADPH to PQ present in the plastoglobules. The PQ pools in the thylakoid and plastoglobules are linked by the outer lipid layer of the thylakoid, which is contiguous with the plastoglobule polar lipid layer. FQR, ferredoxin PQ reductase.

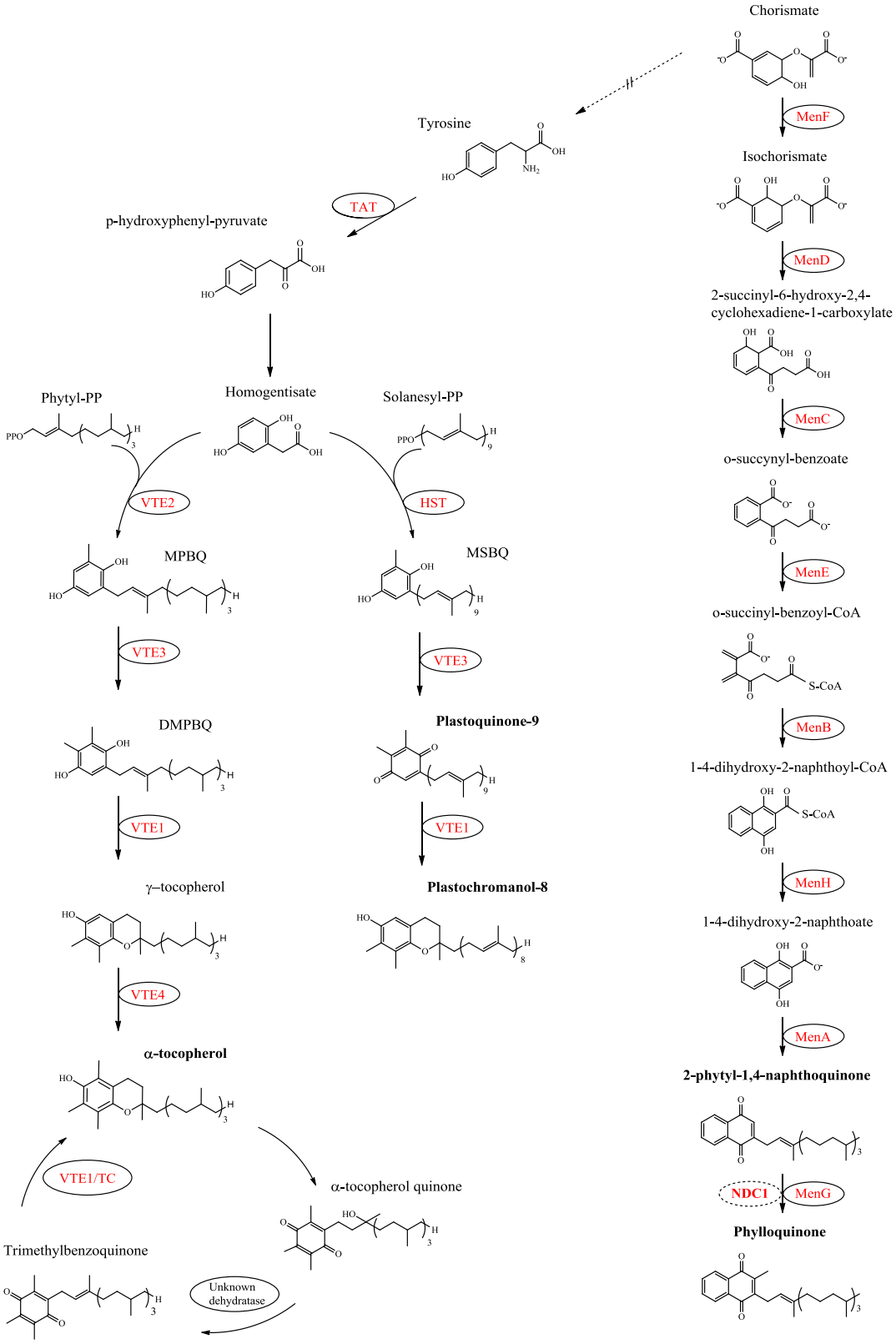

Fig. S2. Biosynthetic pathways of α-tocopherol, PQ, and phylloquinone. The enzyme abbreviations are shown in red. Note that NDC1 is required for the MenG-dependent methylation of 2-phytyl-1,4-naphtoquinone to phylloquinone. DMPBQ, , 2,3-dimethyl-6-phytyl-1,4-benzoquinone; HST, homogentisic acid solanesyl transferase; Men, menaquinone synthesis; MPBQ, 2-methyl-6-phytyl-1,4-benzoquinone; MSBQ, 2-methyl-6-solanesyl-1,4-benzoquinol; -PP, pyrophosphate; TAT, tyrosine aminotransferase; TC, tocopherol cyclase; VTE, vitamin E synthesis.

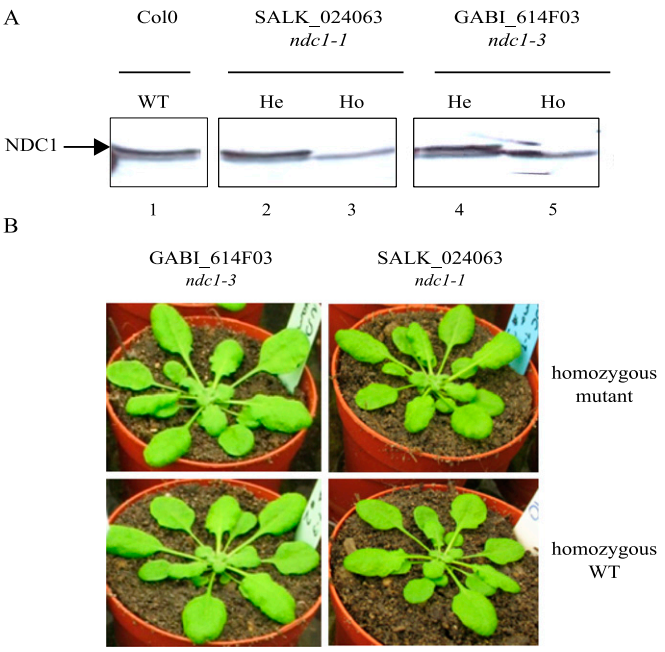

Fig. S3. Isolation of *ndc1* mutant lines. (*A*) Total extracts of two mutant lines, *ndc1-1* and *ndc1-3*, corresponding to 100 μg of protein each were analyzed by Western blotting. Homozygous (Ho) *ndc1-1* (Salk_024063) (lane 3) and *ndc1-3* (GABI_614F03) (lane 5) were null based on the absence of the upper band in the doublet. (*B*) Neither homozygous *ndc1-1* nor *ndc1-3* had a visible phenotype.

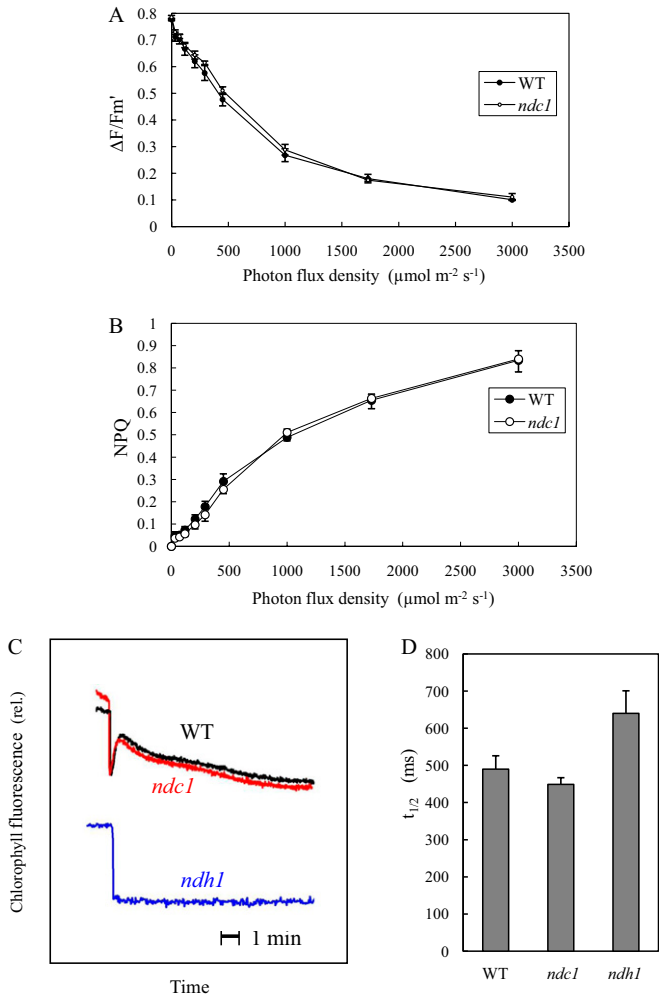

Fig. S4. Photosynthetic properties of WT and *ndc1* mutant leaves of *Arabidopsis*. (*A*) Quantum yield of PSII photochemistry measured at different photon flux densities (PFDs) by using the chlorophyll fluorescence parameter $\Delta F/F_m'$. (*B*) Nonphotochemical energy quenching measured at different PFDs by using the nonphotochemical quenching (NPQ) parameter. Data are mean values of three separate experiments. (*C*) Transient increase in chlorophyll fluorescence after a light-to-dark transition. For comparison purposes, the trace of the *ndh1* mutant is also shown. The data are representative traces of at least five separate experiments. (*D*) Half life $t_{½}$ of the postillumination rereduction of oxidized P700 reduction. Data are mean values of six separate experiments.

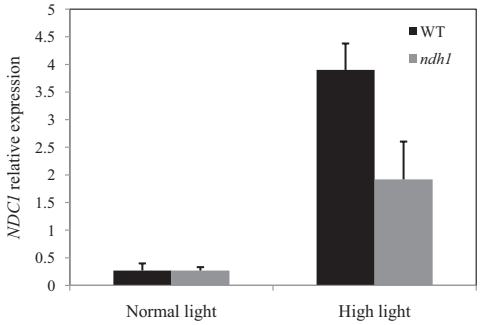

Fig. S5. Analyses of *NDC1* expression in normal and high-light conditions. After extraction of RNA from WT and *ndh1* mutant plants, transcript levels were quantified by real-time RT-PCR with *ACTIN2* as the reference. Values are means of three replicates.

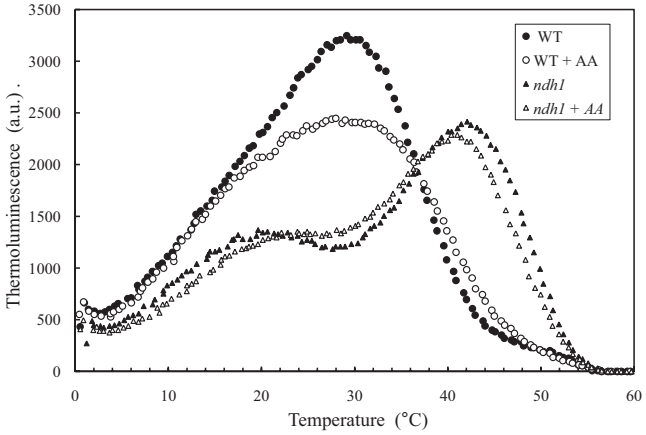

Fig. S6. Effects of 5 μM antimycin A (AA) on the afterglow thermoluminescence band of WT and *ndh1* mutant leaves acclimated for 7 d to high light. Data are representative traces of three separate experiments.

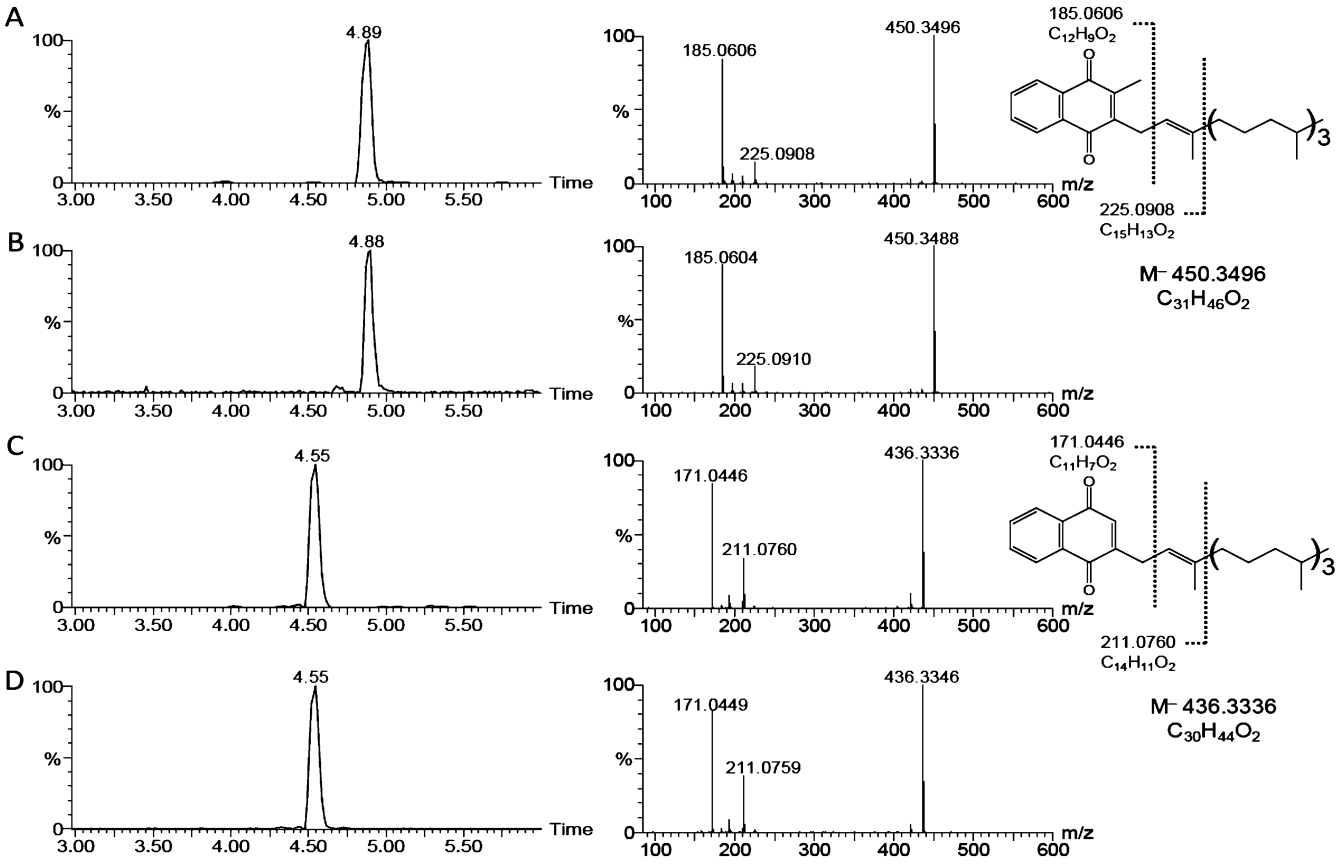

Fig. S7. Extracted ion chromatograms and product ion mass spectra of *m/z* 450.35 and *m/z* 436.33 for phylloquinone standard (*A*), WT extract (*B*), *ndc1-1* extract (*C*), and *AtmenG* extract (*D*).

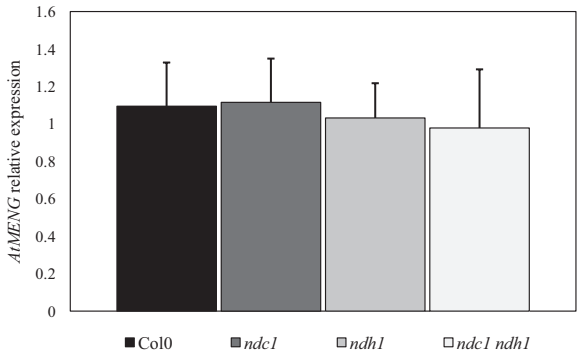

Fig. S8. Analyses of AtMENG expression in *ndc1* mutant lines. Transcript levels were quantified by real-time RT-PCR with *ACTIN2* as the reference. Values are means of three replicates.

Table S1. Data set obtained from ultra HPLC–quadrupole time-of-flight mass spectrometry (UHPLC-QTOFMS) lipidomic analyses of WT and mutant lines

Table S1 (XLSX)

The marker list generated by MarkerLynx XS and PC loadings corresponding to Fig. 4*B* are included.